NANO LETTERS

Letter

pubs.acs.org/NanoLett

Single-Molecule Clocks Controlled by Serial Chemical Reactions

Alexander Johnson-Buck[†,‡,§,∥] and William M. Shih*[,†,‡,§]

[†]Department of Cancer Biology, Dana-Farber Cancer Institute, Boston, Massachusetts 02215, United States

[‡]Wyss Institute for Biologically Inspired Engineering and [§]Biological Chemistry and Molecular Pharmacology, Harvard Medical School, Boston, Massachusetts 02115, United States

Supporting Information

ABSTRACT: Chemical clocks usually achieve well-defined temporal delays through concentration thresholding coupled to the production, degradation, activation, or inhibition of downstream effectors. In this way, the stochastic dynamics of many individual molecules yield essentially deterministic bulk behavior through ensemble averaging. As a result, their temporal evolution is governed by ensemble dynamics rather than by the behavior of an individual molecule or complex. Here, we present a general approach for the design of single-molecule clocks that permits quasi-deterministic control over the lifetime of single molecular interactions without any external synchronization. By coupling the dissociation of a bimolecular complex to a series of irreversible chemical steps, we interpose a well-defined time delay between binding and dissociation. The number and speed of irreversible steps can be varied to systematically tune both the lifetimes of complexes and the precision of the time delay, raising the prospect of localized timekeeping in nanoscale systems and devices.

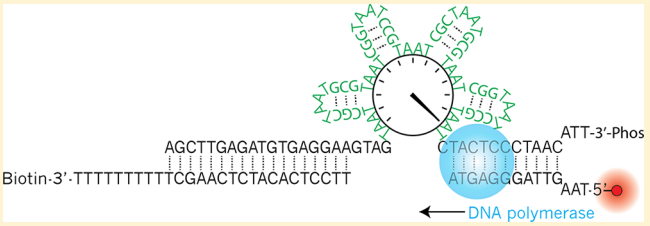

KEYWORDS: *DNA nanotechnology, dynamic DNA nanotechnology, single-molecule, chemical clock, clock reaction, DNA polymerase*

Precise control of the temporal evolution of chemical systems plays important roles in naturally occurring biological systems such as circadian clocks,[1] cardiac pacemaker cells,[2] and embryonic development.[3] Rational engineering of chemical and biochemical kinetics has given rise to systems that mimic some of the features of these natural systems; in addition to classic examples such as the nonoscillatory iodine clock reaction[4,5] and its oscillatory derivatives,[6] synthetic analogs of biological clocks have been constructed in the form of in vitro transcriptional oscillators[7,8] and synthetic oscillatory networks in bacteria.[9] Atomic clocks[10] permit extremely precise analytic timekeeping by spectroscopic determination of resonant frequencies in atoms or ions in the vapor phase. However, it is challenging to achieve precise local control of the time scale of individual molecular events owing to their stochastic dynamics and the typical lack of internal memory. Such control would be valuable, for instance, in permitting the local timing of proposed autonomous molecular devices such as nanoscale assembly lines.[11−13] It may also provide new strategies for multiplexing in fluorescence microscopy, in which transiently binding probes have been used for super-resolution imaging,[14,15] high-confidence identification of endogenous nucleic acids,[16] and precise determination of stoichiometry within biomolecular complexes and aggregates.[17] Here, we outline and experimentally demonstrate a general strategy for precisely controlling the interaction time of single bimolecular complexes. By guiding the complex through a series of several irreversible reactions that terminate in dissociation, it is possible to specify the lifetime of the interaction much more precisely than is achievable for single-step binding or dissociation reactions. We dub such quasi-deterministic devices single-molecule clocks.

The binding equilibrium of a bimolecular complex can usually be approximated as a two-state system whose kinetics are characterized by a bimolecular association rate constant, k_0, and a unimolecular dissociation rate constant, k_1 (Figure 1a). Thus, when the reversible binding of a fluorescent probe to an immobilized target[14] is monitored at the single-molecule level, the dwell times in the high-fluorescence (bound) state are exponentially distributed (Figure 1a). The complex has no memory of how long it has existed, and its probability of dissociating within an interval of time Δt is independent of its history, resulting in a broad range of complex lifetimes (coefficient of variation equal to 1 in the ideal case). In contrast, single-molecule clocks pass through a series of intermediates via irreversible reactions characterized by rate constants k_1, k_2,...k_N before dissociation can occur (Figure 1b). While the dwell time τ_i of each intermediate is a random value drawn from an exponential distribution, the overall wait time is:

$$\Delta t = \sum_{i=1}^{N} \tau_i \tag{1}$$

It follows a gamma distribution, with a coefficient of variation proportional to $1/\sqrt{N} < 1$ (Figure 1b).[18] That is, as the number of irreversible steps increases, the lifetime of the

Received: October 10, 2017
Revised: October 31, 2017
Published: November 1, 2017

DOI: 10.1021/acs.nanolett.7b04336
Nano Lett. 2017, 17, 7940−7944

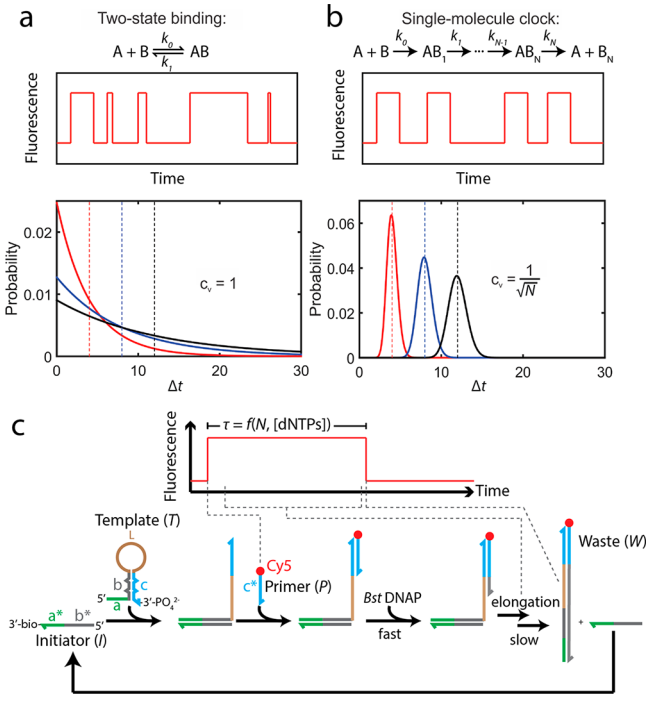

Figure 1. Principles and implementation of single-molecule clocks. (a) The equilibrium two-state binding of a conventional probe (as in DNA-PAINT) results in a wide range of bound-state dwell times that follow an exponential distribution whose coefficient of variation (σ/τ) is equal to 1. Complexes with τ = 4, 8, and 12 s (red, blue, and black lines, respectively) are predicted to have substantial overlap in their Δt distributions. (b) A single-molecule clock exploits a series of irreversible chemical steps that must occur between binding and dissociation of the probe, resulting in a gamma distribution of dwell times whose coefficient of variation is $1/\sqrt{N}$, where N is the number of irreversible steps. Clock complexes with N = 40, 80, and 120, and τ = 4, 8, and 12 s (red, blue, and black lines, respectively) are predicted to have Δt distributions that only minimally overlap. (c) Implementation of single-molecule clocks using a DNA polymerase (DNAP) with strand displacement activity. A hairpin-loop template (T) binds to an initiator (I) via toehold-mediated strand displacement, revealing the primer-binding domain c. Binding of the fluorescent primer (P) yields a localized increase in fluorescence and is rapidly followed by the binding of DNAP. Elongation of the primer by DNAP serves as the rate-limiting process for dissociation and results in the displacement of I from the fluorescent waste complex (W), which diffuses away and results in a loss of fluorescence. As long as elongation is slow relative to DNAP binding, the duration of the localized spike in fluorescence is controlled (or clocked) by the stepwise addition of deoxyribonucleoside triphosphates (dNTPs) to the growing DNA strand. Note that the duplex stem of T contains two mismatched base pairs that are introduced to ensure orthogonal binding between sequences b/b* and c/c* (i.e., to prevent binding of P directly to I).

complex becomes more narrowly distributed relative to its expectation value or more deterministic.

Although the single-molecule clock principle might be implemented in various ways, one of the most convenient and compact approaches is to use a processive enzyme such as a DNA polymerase (DNAP). We therefore constructed a system in which a DNAP with strand displacement activity controls the delay between the binding and dissociation of a fluorescent probe (Figure 1c). An initiator strand I binds to a hairpin template T (Figure S1), opening the hairpin and exposing a primer binding site on T. Subsequently, a fluorophore-labeled primer P binds to the complex, resulting in an increase in localized fluorescence. Almost immediately (because [DNAP] > 1 μM), the DNAP binds and begins elongating the primer. Upon reaching the end of the template, the strand displacement activity of the DNAP causes the fluorescent waste complex W to dissociate from I, resulting in a loss of fluorescence from the binding site. The dwell time in the high-fluorescence state is thus controlled by the rate of nucleotide addition and is expected to exhibit a gamma distribution of dwell times whose shape and mean value is dependent on the length of the template and the concentration of dNTPs. Because clock behavior requires that polymerase binding is fast relative to polymerization, we performed a kinetic assay by polyacrylamide gel electrophoresis to confirm this fact (Figure S2).

To characterize clock behavior at the single-molecule level, we used a total internal reflection fluorescence (TIRF) assay in which biotinylated initiator strand I was immobilized on a passivated coverslip (Figure 2b; see the description of the methods for details). In this scheme, repeated cycles of increased and decreased fluorescence intensity are expected to occur at the position of each surface-immobilized copy of I, with the duration of each burst controlled by polymerase activity. Such repeated fluorescence bursts are indeed observed (Figure 2c), and as expected, exhibit a narrow, nonexponential distribution of dwell times (Δt) in the bound state (Figure 2d). Fitting a gamma probability distribution to the Δt histogram yields a mean dwell time $\overline{\Delta t}$ of 12.7 ± 0.2 s for a 41-nucleotide template (T_{41}). Importantly, the photobleaching lifetime (determined in the absence of dNTPs or polymerase) is ~83.8 s (Figure S3); thus, only ~15% of primers are expected to photobleach before dissociating under these conditions. Consistent with the hypothesis that dwell time is predominantly controlled by the rate of nucleotide addition, $\overline{\Delta t}$ is strongly dependent on the concentration of dNTPs (Figure 2e), exhibiting saturation behavior with an apparent Michaelis constant (K_M) of 12.6 ± 2.4 μM with respect to dNTPs, consistent with a previous estimate.[19] Notably, a minority of events exhibit much longer dwell times, which may be due to nonspecific binding of probes to the imaging surface or occasional polymerase stalling (Figure S4).

Because the number of irreversible steps between binding and dissociation increases, two trends are expected: (i) $\overline{\Delta t}$ should increase in proportion to template length, and (ii) dwell time distributions should have a smaller coefficient of variation. To test these predictions, we constructed a set of templates with identical toehold and stem domains but with varying length of the terminal loop, with total lengths ranging from 41 to 153 nucleotides (Figure 3a–d). For longer loops, short hairpins were intentionally introduced to prevent unwanted base-pairing between the stem and terminal loop and to reduce the entropic penalty for loop closure. As expected, in the presence of a saturating concentration (100 μM) of dNTPs, all templates exhibited repeated bursts of fluorescence with a precisely determined Δt that increased with template size (Figure 3a–d). Notably, several of the Δt distributions are well-separated from one another (Figure 3e), making it possible in principle to distinguish between templates from the duration of only one binding event. Fitting a gamma distribution to the main peak of each dwell time histogram yields estimates of $\overline{\Delta t}$ that depend linearly on the length of the template (Figure 3f), providing further evidence that polymerization is the primary rate-limiting process prior to complex dissociation. The slope of

DOI: 10.1021/acs.nanolett.7b04336
Nano Lett. 2017, 17, 7940–7944

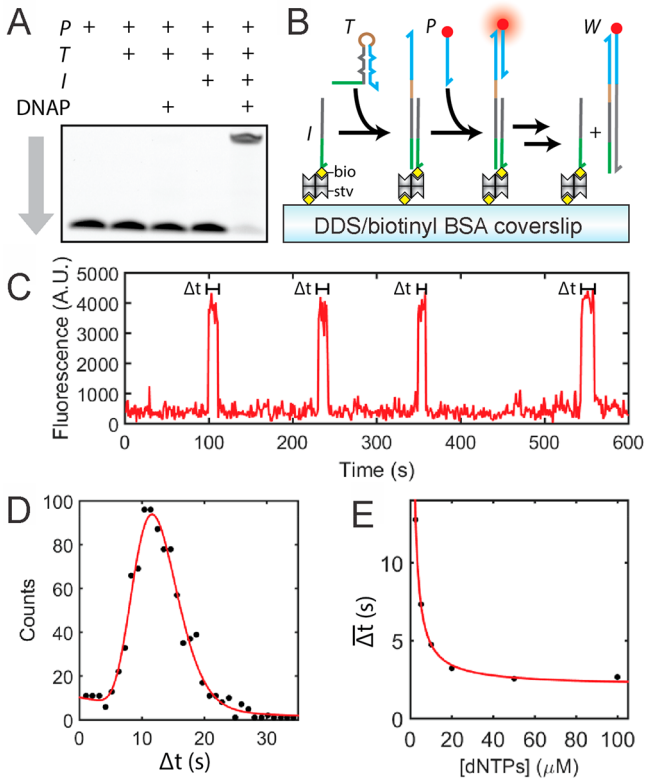

Figure 2. Demonstration of a polymerase-controlled single-molecule clock. (a) Denaturing polyacrylamide gel showing the DNAP-catalyzed extension of a Cy5-labeled primer (P) in the presence of a 41-nucleotide (nt) loop template, T_{41}. Extension of the Cy5-labeled primer occurs efficiently only in the presence of T_{41}, initiator (I), and DNAP. No detectable leakage occurs in the absence of I. Incubation time: 5 min. Gray arrow indicates the direction of migration in the gel. (b) Surface-based assay of single-molecule clock performance using total internal reflection fluorescence microscopy. Each surface-anchored copy of I undergoes repeated cycles of T_{41} binding, P binding, extension by DNAP, and displacement of W. Localized fluorescence is only visible between binding of P and the dissociation of W. (c) Representative single-molecule fluorescence trajectory showing four consecutive clock binding cycles in the same location on a coverslip using T_{41}. (d) Dwell time distribution for T_{41} in the presence of 2.5 μM dNTPs (n = 1000 binding events). The red line represents a nonlinear least-squares fit of a gamma probability distribution to the data, yielding an estimated mean dwell time, $\overline{\Delta t}$, of 12.7 ± 0.2 s (95% confidence bounds from fit). (e) Dependence of the mean dwell time on dNTP concentration. The red line represents a nonlinear least-squares fit of a Michaelis–Menten saturation curve to the data, resulting in an estimated K_M of 12.6 ± 2.4 μM and a τ_{min} of 2.1 ± 0.3 s (95% confidence bounds from fit).

a linear fit yields an estimated elongation rate of ~8.3 nt s^{-1}, considerably slower than the maximum elongation rate of 191.2 nt s^{-1} reported for this polymerase at 65 °C[20] but much faster than the maximum rate of 0.047–0.24 nt s^{-1} reported at room temperature using coumarin-modified dNTPs[19] (all experiments in the present study were performed at room temperature using unmodified dNTPs). In addition to $\overline{\Delta t}$, fitting of a gamma distribution to the experimental Δt histograms yields estimates of N_{app}, the apparent number of irreversible steps between binding and dissociation, and $\overline{\Delta t_{step}}$, the apparent average dwell time per step. As expected, N_{app} increases linearly with the length of the template (Figure S5), indicating more deterministic behavior as the number of steps increases. However, contrary to naïve predictions, N_{app} is not equal to the number of nucleotides added but is related by a proportionality constant of ~0.43, suggesting that not all nucleotide addition steps are equally rate-limiting. Perhaps the simplest explanation for this higher-than-predicted N_{app} is that different dNTPs are incorporated with substantially different kinetics, which has been observed experimentally for Klentaq polymerase.[21] Using Monte Carlo simulations, we find that a value of N_{app}/N = 0.43 is obtained if one of the nucleotides is incorporated at a rate 9-fold lower than the other three nucleotides, for instance (Figure S6). The apparent number of steps could also be diminished by dissociation of the waste complex before the polymerase reaches the end of the template or by partially rate-limiting polymerase binding and initiation kinetics. However, $\overline{\Delta t_{step}}$ is essentially constant across all studied template lengths (Figure S5), consistent with expectations that the rate of polymerization is independent of the length of the template. As expected, the dwell times in the unbound state are not clocked and follow a simple exponential distribution (Figure S7).

We have demonstrated one way of implementing single-molecule clocks (namely, using DNA polymerases with strand-displacement activity). We have further shown that the quasi-deterministic temporal behavior of this class of single-molecule clocks can be systematically tuned by varying the length of the template and the rate of polymerization. Historically, the term "chemical clock" has been applied to both nonoscillatory[4,5,22] systems, in which an initial induction period is followed by a sudden change in reagent concentration,[23] and oscillatory[6] systems, in which the concentration of a reagent undergoes repeated changes in concentration with a well-defined period. While we only demonstrate implementation of a nonoscillatory single-molecule clock here, the principle of generating time delays through serial reactions may be used to design periodic single-molecule clocks in the future, provided that sufficiently well-behaved systems (i.e., devoid of significant kinetic traps) are discovered or designed.

While we have exploited DNA polymerization as the source of serial reactions, in principle, any series of irreversible reactions with similar kinetics could be substituted for the polymerization as long as they control the time interval between two reporting events. For example, DNA-only catalytic cascades,[24] as well as RNA polymerases, exonucleases, ATP-dependent helicases, and other processive enzymes that act upon templates of well-defined size, may be expected to yield single-molecule clock behavior. In some cases, such systems may even function as clocks in their native biological contexts as, for example, has been hypothesized for translational pausing in protein folding.[25]

In the future, a number of improvements and modifications on this principle may be possible. In our system, a background of exponentially distributed binding events is evident in the dwell time histograms and becomes more dominant for templates of increasing length (Figures 3e and S4), possibly due to polymerase stalling, which is expected to occur in a larger fraction of templates as the number of base pairs per template increases. Improved template sequence design and alternate polymerases may reduce the influence of polymerase stalling on dwell time distributions, resulting in higher-fidelity clocks. While the clocks presented in this manuscript exhibit bound-state lifetimes in the range of ~1–20 s, these may be lengthened (e.g., by lowering dNTP concentration or

DOI: 10.1021/acs.nanolett.7b04336
Nano Lett. 2017, 17, 7940–7944

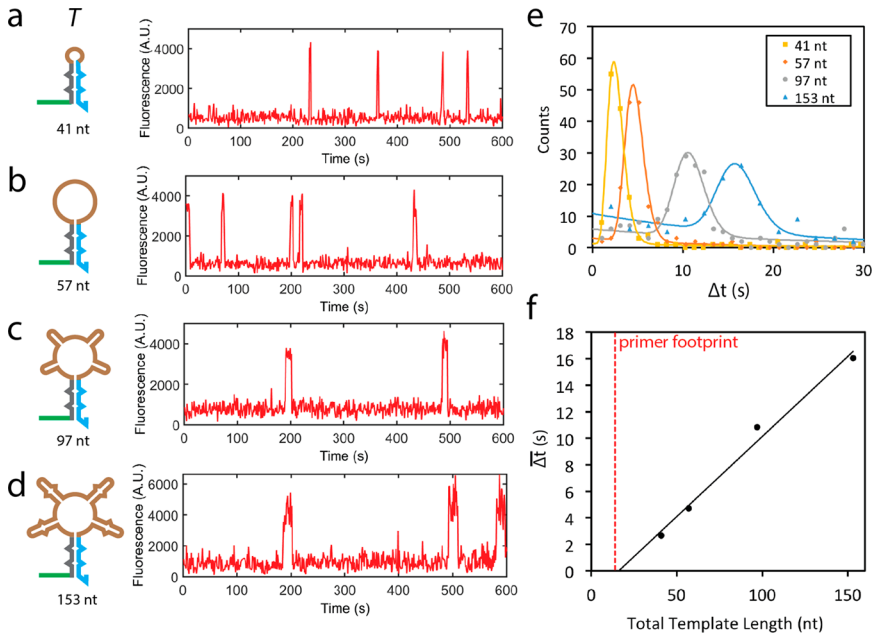

Figure 3. Design of polymerase-clocked clocks with tunable duration. (a–d) Design schematics (left) and representative single-molecule fluorescence traces (right) of clocks using four different templates (T) of varying loop length. The indicated number of nucleotides (nt) is the total length of each template, including the constant primer- and initiator-binding domains. (e) Dwell time distributions and gamma probability distribution fits for the four clock templates shown in panels a–d. Binding events (n = 143, 154, 196, and 155) occurred for the 41, 57, 97, and 153 nt templates, respectively. (f) Dependence of mean dwell time on total template length. A linear regression fit to the data is shown; slope = 0.12 s nt^{-1} and R^2 = 0.986. The red dashed line indicates the 14 nt footprint of the primer binding site on the template, which does not contribute to the timing mechanism. All experiments shown in this figure were performed in the presence of a saturating concentration (100 μM) of dNTPs.

increasing template length) or shortened (e.g., by lowering monovalent ion concentration to increase the elongation rate of the polymerase) to suit the needs of a given application. In addition, the further development of polymerases that act upon bio-orthogonal nucleotide analogs may ensure greater compatibility with a variety of applications in biological imaging and biomolecular nanotechnology. We anticipate a variety of compelling uses for the deterministic control of kinetics at the single-molecule level.

■ ASSOCIATED CONTENT

Supporting Information

The Supporting Information is available free of charge on the ACS Publications website at DOI: 10.1021/acs.nanolett.7b04336.

Additional details on materials and methods including protocols for TIRF microscopy, denaturing polyacrylamide gel electrophoresis assays, kinetic analysis of single-molecule data, and Monte Carlo simulations as well as a list of oligonucleotide sequences used for single-molecule clocks and figures showing secondary structures, ensemble time courses, photobleaching kinetics, cumulative dwell time distributions, distribution parameters, and Monte Carlo simulation results. (PDF)

■ AUTHOR INFORMATION

Corresponding Author

*E-mail: William_Shih@dfci.harvard.edu. Phone: 617-632-5143. Fax: 617-394-2897.

ORCID

William M. Shih: 0000-0002-1395-9267

Present Address

‖A.J.-B.: Department of Internal Medicine, The University of Michigan, Ann Arbor, MI 48109, United States

Notes

The authors declare the following competing financial interest(s): The Harvard University Office of Technology Development has filed a provisional patent application on technologies described herein.

■ ACKNOWLEDGMENTS

The Harvard University Office of Technology Development has filed a provisional patent application on technologies described herein. This work was funded by support from NSF Expeditions award no. CCF-1317291, NSF DMREF award no. 1435964, ARO MURI award no. W911NF-12-1-0420, ONR award no. N000141510073, the Dana Farber Cancer Institute Claudia Adams Barr Award, the Harvard Catalyst Pilot Grant Award, and the Wyss Institute at Harvard Faculty Award to W.M.S.

■ REFERENCES

(1) Harmer, S. L.; Hogenesch, J. B.; Straume, M.; Chang, H.-S.; Han, B.; Zhu, T.; Wang, X.; Kreps, J. A.; Kay, S. A. *Science* **2000**, *290*, 2110–2113.
(2) Glass, L. *Nature* **2001**, *410*, 277–284.
(3) Pourquié, O. *Science* **2003**, *301*, 328–330.
(4) Landolt, H. *Ber. Dtsch. Chem. Ges.* **1886**, *19*, 1317–1365.
(5) Oliveira, A. P.; Faria, R. B. *J. Am. Chem. Soc.* **2005**, *127*, 18022–18023.
(6) Briggs, T. S.; Rauscher, W. C. *J. Chem. Educ.* **1973**, *50*, 496.
(7) Kim, J.; Winfree, E. *Mol. Syst. Biol.* **2011**, *7*, 465.
(8) Baccouche, A.; Montagne, K.; Padirac, A.; Fujii, T.; Rondelez, Y. *Methods* **2014**, *67*, 234–249.
(9) Elowitz, M. B.; Leibler, S. *Nature* **2000**, *403*, 335–338.

DOI: 10.1021/acs.nanolett.7b04336
Nano Lett. 2017, 17, 7940–7944

(10) Essen, L.; Parry, J. V. L *Nature* **1955**, *176*, 280−282.
(11) He, Y.; Liu, D. R. *Nat. Nanotechnol.* **2010**, *5*, 778−782.
(12) Gu, H.; Chao, J.; Xiao, S.-J.; Seeman, N. C. *Nature* **2010**, *465*, 202−205.
(13) Kassem, S.; Lee, A. T. L.; Leigh, D. A.; Markevicius, A.; Solà, J. *Nat. Chem.* **2015**, *8*, 138−143.
(14) Jungmann, R.; Steinhauer, C.; Scheible, M.; Kuzyk, A.; Tinnefeld, P.; Simmel, F. C. *Nano Lett.* **2010**, *10*, 4756−4761.
(15) Jungmann, R.; Avendaño, M. S.; Woehrstein, J. B.; Dai, M.; Shih, W. M.; Yin, P. *Nat. Methods* **2014**, *11*, 313−318.
(16) Johnson-Buck, A.; Su, X.; Giraldez, M. D.; Zhao, M.; Tewari, M.; Walter, N. G. *Nat. Biotechnol.* **2015**, *33*, 730−732.
(17) Jungmann, R.; Avendaño, M. S.; Dai, M.; Woehrstein, J. B.; Agasti, S. S.; Feiger, Z.; Rodal, A.; Yin, P. *Nat. Methods* **2016**, *13*, 439−442.
(18) Floyd, D. L.; Harrison, S. C.; van Oijen, A. M. *Biophys. J.* **2010**, *99*, 360−366.
(19) Walsh, M. T.; Roller, E. E.; Ko, K.-S.; Huang, X. *Biochemistry* **2015**, *54*, 4019−4021.
(20) Kiefer, J. R.; Mao, C.; Hansen, C. J.; Basehore, S. L.; Hogrefe, H. H.; Braman, J. C.; Beese, L. S. *Structure* **1997**, *5*, 95−108.
(21) Montgomery, J. L.; Rejali, N.; Wittwer, C. T. *J. Mol. Diagn.* **2014**, *16*, 305−313.
(22) Forbes, G. S.; Estill, H. W.; Walker, O. J. *J. Am. Chem. Soc.* **1922**, *44*, 97−102.
(23) Preece, S. J.; Billingham, J.; King, A. C. *J. Math. Chem.* **1999**, *26*, 47.
(24) Yin, P.; Choi, H. M. T.; Calvert, C. R.; Pierce, N. A. *Nature* **2008**, *451*, 318−322.
(25) Marin, M. *Biotechnol. J.* **2008**, *3*, 1047−1057.

DOI: 10.1021/acs.nanolett.7b04336
Nano Lett. 2017, 17, 7940−7944